MIKAILALSYS
Journal of Multidisciplinary Sciences

e-ISSN : 2987-2286
p-ISSN : 2987-3924
Index: Harvard, Boston, Sydney, Copernicus, Sinta 4, Scilit, Semantic, Google, etc

https://doi.org/10.58578/mikailalsys.v4i3.12540

# Experimental Validation of End-Effector Position Accuracy and Repeatability of a Waste-Sorting Delta Robot

**Lukas E. Hasibuan, Yohandri, Zulhendri Kamus, Mona Berlian Sari**
Universitas Negeri Padang, Indonesia
qweerwin12@gmail.com

| Submitted: | Revised: | Accepted: | Published: |
|---|---|---|---|
| Sep 21, 2026 | Oct 20, 2026 | Oct 31, 2026 | Nov 5, 2026 |

**Abstract**

The positioning accuracy of Delta robots depends on the agreement between the kinematic model and actual arm motion, particularly in systems driven by open-loop stepper motors with belt transmissions. This study experimentally validated a simplified kinematic model for a waste-sorting Delta robot by evaluating angular accuracy and end-effector distance precision and repeatability. A closed-form inverse kinematics model was formulated to map target coordinates to arm angles and stepper microsteps and implemented on an Arduino Mega 2560. Angular accuracy was assessed by comparing model-computed arm angles with digital inclinometer measurements at three target points corresponding to waste-bin locations, with 10 repetitions per point. Distance precision and repeatability were evaluated through 10 repeated movements between two points 82 mm apart, with pen-marked positions measured using ImageJ. The results showed a mean angular accuracy of 98.71%, a mean distance precision of 99.88%, and distance repeatability of ±0.39 mm. Angular errors were systematic and varied across arms, with the largest mean error of 1.72° observed in arm 2. The end-effector displacement estimated from these errors ranged from 3.6 to 5.8 mm, remaining below the 25 mm radius of the waste-bin opening. These findings provide experimental support for the feasibility of the simplified kinematic model for waste placement at the tested positions and indicate potential for improving positioning accuracy through per-arm error compensation.

**Keywords:** Delta Robot; Inverse Kinematics; Positioning Accuracy; Repeatability; Waste Sorting


Mikailalsys is licensed under a Creative Commons Attribution-NonCommercial-ShareAlike 4.0 International License

## INTRODUCTION

Automated waste sorting requires robots that can recognize waste categories and accurately transfer them from a conveyor to their destination containers. Kiyokawa et al. (2024) identified three main challenges for robotic waste sorters: reliable end effectors for dirty and deformable objects, sensors for recognizing object categories and poses, and feasible and efficient motion planners. Computer vision has become the main approach for identifying waste in automated sorting, with a clear shift from traditional machine learning to deep learning (Lu & Chen, 2022), and artificial intelligence is increasingly applied across the waste management cycle (Fang et al., 2023). Nevertheless, most automatic waste separation systems reported in the literature are still evaluated in laboratory environments (Arbeláez-Estrada et al., 2023), and commercial sorting technology still has difficulty with certain items such as black plastics and films (Lubongo & Alexandridis, 2022). These three challenges are interdependent. Accurate object detection is of no use if the manipulator cannot place the end effector precisely at the detected coordinates.

Delta robots are widely chosen for high-speed pick-and-place tasks because of their parallel structure. This robot was developed by Clavel (1988) and consists of three identical kinematic chains connecting a fixed base to a moving platform, so that the platform only translates and always remains parallel to the base (Pierrot et al., 1990). The actuators are mounted on the base, which keeps the moving mass light and allows the robot to reach high accelerations. The geometric, kinematic, and dynamic analyses of the Delta robot have also been formulated as iterative matrix relations (Staicu & Carp-Ciocardia, 2003), so its mathematical model is relatively well established. Vision-guided Delta robots have since been applied to pick-and-place and sorting tasks, including a Delta robot controlled through YOLOv5-based visual servoing (Yamtuan et al., 2023) and a vision-supported pick-and-place Delta robot (Elassal et al., 2024), in line with the broader growth of vision-based robotic applications (Shahria et al., 2022).

Although its kinematic model is well established, the positioning accuracy of a physical robot still depends on how closely the actual geometric parameters match the nominal values in the model. Bai et al. (2016) modeled the sources of geometric error in a Delta robot, identified them using distance measurements with a laser tracker, and showed that positioning accuracy could be substantially improved through compensation. Such calibration approaches have been applied to prototypes with a repeatability of about 0.05

mm and require expensive measuring instruments (Bai et al., 2016). Error analyses of Delta mechanisms show that geometric parameter errors, joint clearance, and actuator driving errors all propagate to the end-effector position (Yang et al., 2021), calibration methods originally developed for serial robots have been extended to the Delta robot (Bentaleb & Iqbal, 2020), and the positioning accuracy of robots is increasingly treated as a reliability problem under parameter uncertainty (Cao et al., 2023). These conditions differ from those of a Delta robot driven by stepper motors and belt transmissions, such as the one used in this study.

Some Delta robots use stepper motors instead of AC servo motors, such as the design of Phuong et al. (2023), which combined a Delta robot with a vision system to pick objects from a conveyor. Using stepper motors simplifies the control system but introduces characteristic sources of error. Stepper motors are usually controlled in open loop, so steps lost due to overloading are not detected by the controller, and the actual position deviates from the assumed position (Moon & Kim, 2014). Such position errors in open-loop microstepping operation can be reduced, for example, by optimizing the drive waveforms (Pillans, 2021). In addition, the belt and pulley transmissions used to increase torque can introduce backlash and compliance, while the microstepping resolution does not necessarily reflect the actual angular accuracy. Timing belt drives exhibit transmission errors caused by elasticity, backlash, and slip between the belt and the pulleys (Kılıç et al., 2010, 2012), and recent measurements on a belt-driven positioning system confirmed that belt elasticity and micro-slip contribute to the final positioning deviation (Tornai et al., 2025).

Some validations of stepper-driven Delta robots still rely on task success, for example the success of picking objects from a conveyor (Phuong et al., 2023). Such measures are influenced by object size and gripper tolerance, so they do not show how closely the end-effector displacement matches the value commanded by the model. Accuracy expresses the closeness of a measurement result to a reference value, whereas precision expresses the closeness among repeated measurement results under the same conditions (Joint Committee for Guides in Metrology, 2012). Precision measured under fixed test conditions is also called repeatability (Joint Committee for Guides in Metrology, 2012). Testing robot accuracy with instruments such as a laser tracker (Bai et al., 2016) is difficult to implement in educational laboratories, so a test procedure that can be carried out with simple measuring instruments is needed.

This study is part of a waste-sorting robot system based on YOLOv5 object detection that uses a Delta robot. The robot is driven by three NEMA 17 stepper motors with a 3:1 belt transmission and 1/16 microstepping, controlled in open loop. In this system, the coordinates of objects obtained from detection are corrected for conveyor displacement before being sent to the robot, so the success of sorting depends directly on how accurately the robot reaches the commanded coordinates. This study aims to formulate a simplified kinematic model that maps target coordinates into the number of stepper microsteps, and then to validate it experimentally through an arm-angle accuracy test at three waste-bin positions and an end-effector position precision test.

The contribution of this study is twofold. First, the closed-form inverse kinematics model of the Delta robot is complemented by an angle-to-microstep conversion that accounts for the transmission ratio and microstepping. Second, the model is validated with a simple test procedure using a digital inclinometer and pen marks on paper, so that the accuracy and precision of the robot can be expressed quantitatively. The Methods section describes the materials and methods, the Results and Discussion sections present the findings and their interpretation, and the Conclusion section summarizes the study.

## METHODS

This study was an experimental study with a quantitative approach. Experimental research tests the effect of a treatment on an outcome while controlling other factors that may influence that outcome, whereas a quantitative approach examines relationships among variables that can be measured with instruments, producing numerical data that are analyzed statistically (Creswell & Creswell, 2018). In this study, the treatment was the target coordinates given to the robot as the independent variable, while the measured arm angles and end-effector positions were the dependent variables. The control variables included movement speed, acceleration, safe height, direction of motion, the pen, and the Arduino Mega microcontroller and A4988 drivers. The arm angles read by the digital inclinometer were used as reference values, so accuracy was determined by comparing the arm angles computed by the code with these measured angles.

### System Design

The Delta robot used in this study consists of a 12 V power supply, an Arduino Mega 2560 as the controller, a RAMPS (RepRap Arduino Mega Pololu Shield) 1.6 shield, three

A4988 drivers, three NEMA 17 stepper motors, and three limit switches. Its mechanical part consists of a frame, a base, three upper arms, three pairs of lower arms, and an end effector. The relationships among these components are shown in the system block diagram in Figure 1.

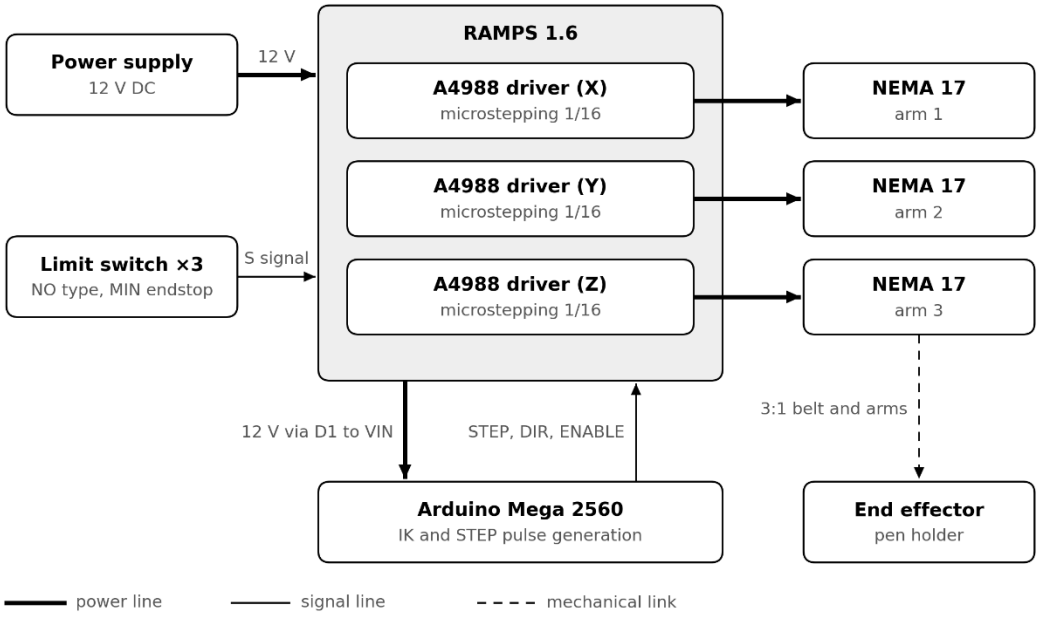



**Figure 1. System Block Diagram of the Delta Robot**

Figure 1 shows that the 12 V power supply powers the RAMPS 1.6, which distributes power to the three A4988 drivers as well as to the Arduino Mega 2560 (RepRap, n.d.). The Arduino Mega 2560 computes the arm angles from the target coordinates and then sends the STEP, DIR, and ENABLE signals to each driver through the RAMPS. Each STEP pulse rotates the motor by one microstep in the 1/16 microstepping mode, while the DIR signal level determines the direction of rotation (Allegro MicroSystems, 2022). The three limit switches are the only feedback in the system and are used solely during homing to set the reference position of the arms. The motor rotation is transmitted to the upper arms through a belt transmission, so that the three arms together move the end effector. The physical arrangement of these components on the robot frame is shown in the hardware design in Figure 2.

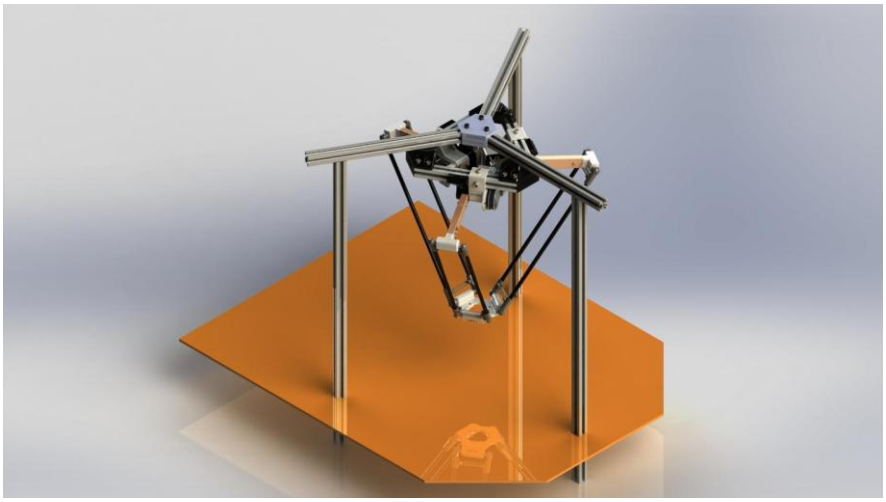


**Figure 2. Hardware Design of the Delta Robot**

Figure 2 shows the hardware design of the Delta robot. The robot frame consists of three vertical legs and three horizontal bars made of aluminum profiles that meet at the center, where the robot base is mounted. The three stepper motors are mounted on the base and rotate the upper arms through a 20-tooth pulley on the motor shaft and a 60-tooth pulley on the arm, giving a reduction ratio of 3:1. Each upper arm is connected to the end effector through a pair of lower-arm rods forming a parallelogram, which are held together by springs at their joints. The plate at the bottom of the frame serves as the work surface on which the test paper is placed during testing. The geometric and transmission parameters of the robot are summarized in Table 1.

**Table 1. Geometric and Transmission Parameters of the Delta Robot**

| Parameter | Symbol | Value |
|---|---|---|
| Base triangle side | $s_B$ | 265 mm |
| End-effector triangle side | $s_E$ | 120 mm |
| Upper arm length | $L_1$ | 130 mm |
| Lower arm length | $L_2$ | 316 mm |
| Motor full-step angle | $a_s$ | 1.8° |
| Microstepping factor | $\mu$ | 16 |
| Belt transmission ratio | $G$ | 3 (60:20) |

Table 1 shows that the resolution of arm motion is determined by the motor full-step angle, the microstepping factor, and the belt transmission ratio. These three parameters are used in the conversion of arm angles into microsteps, while the geometric parameters are used in the simplified kinematic model. The program sequence on the Arduino Mega 2560, from the moment the robot is switched on until the end effector completes one motion cycle, is shown in the flowchart in Figure 3.

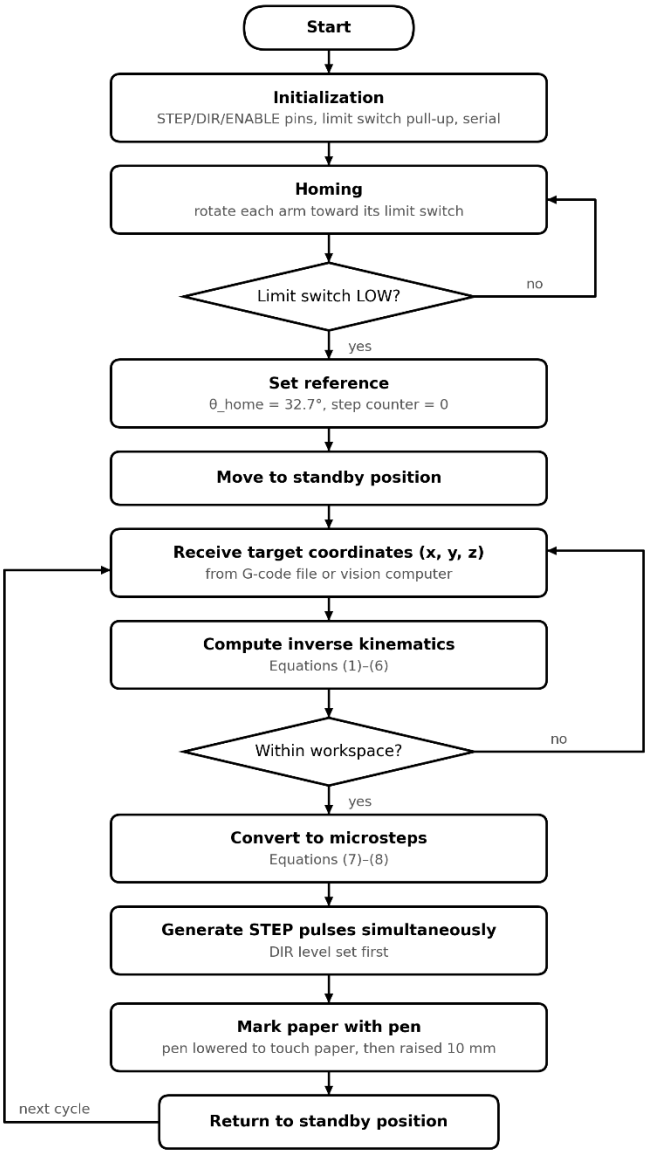



**Figure 3. Program Flowchart of the Delta Robot**

Figure 3 shows that the program begins with pin initialization and homing, in which each arm is rotated toward its limit switch until its reference position is obtained. The end effector then moves to the standby position, and the program waits for target coordinates from a G-code file containing the list of test points or from the vision computer. These coordinates are processed using inverse kinematics in Equations (1)–(6), and targets outside the workspace are rejected. The computed angles are converted into the number of microsteps using Equations (7) and (8), and STEP pulses are then generated simultaneously for the three arms. After the target point is reached, the pen is lowered until it touches the paper and then raised again, after which the end effector returns to the standby position for the next cycle.

**Simplified Kinematic Model**

The model was developed under five simplifying assumptions. First, all arms are assumed to be rigid. Second, all joints are assumed to be ideal without clearance. Third, each pair of parallelogram lower arms is represented by a single rod of length $L_2$, as done by Pierrot et al. (1990). Fourth, the three arms are arranged symmetrically at 120° intervals. Fifth, all geometric parameters are equal to their nominal values. These assumptions allow the model to be solved in closed form, but they also neglect manufacturing errors, joint compliance, backlash, and friction, which according to Zhao et al. (2023) make geometry-based inverse kinematics of stepper-driven Delta robots not entirely accurate.

The coordinate frame $O$–$xyz$ is placed at the center of the base triangle with the $z$-axis pointing upward, so that the workspace lies at negative $z$ (Figure 4). Because the motors are mounted at the midpoints of the triangle sides, the distance from the motor axis to the center of the base and the distance from the end-effector joint to its center are equal to the inradius of the respective triangles:

$$R = \frac{s_B}{2\sqrt{3}}, \qquad r = \frac{s_E}{2\sqrt{3}} \tag{1}$$

The positions of these geometric quantities in the working plane of arm 1 are shown in Figure 4. This schematic serves as the reference for deriving the arm-angle equations below. Arms 2 and 3 have the same arrangement after their working planes are rotated by 120° and 240°.

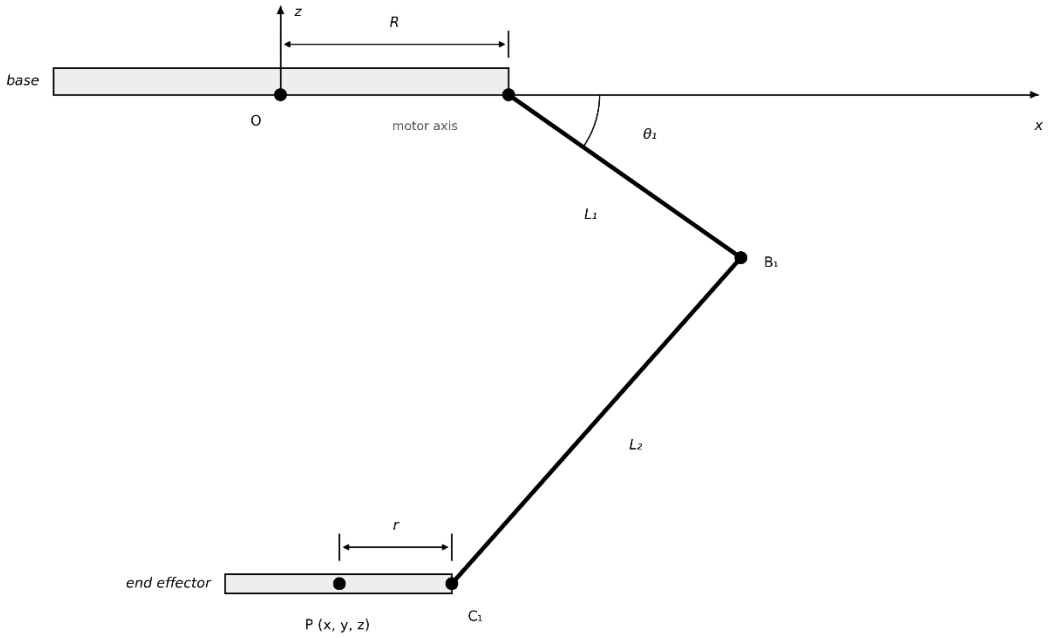



**Figure 4. Geometric Schematic of the Delta Robot in the Working Plane of Arm 1: Base Coordinate Frame O–xyz, Radii R and r, Upper Arm Length $L_1$ and Lower Arm Length $L_2$, Elbow Point $B_1$, End-Effector Joint Point $C_1$, and Arm Angle $\theta_1$**

The derivation starts with arm 1, which lies in the $xz$-plane. The elbow point of arm 1, $B_1$, is located at $(R + L_1 \cos\theta_1, 0, -L_1 \sin\theta_1)$, where $\theta_1$ is the angle of the upper arm relative to the horizontal plane, positive downward. For an end-effector center position $P = (x, y, z)$, the joint of the lower arm on the end effector, $C_1$, is located at $(x + r, y, z)$. The lower arm has a fixed length, so the distance from $B_1$ to $C_1$ is always equal to $L_2$. In squared form, this condition is written as

$$(x + r - R - L_1\cos\theta_1)^2 + y^2 + (z + L_1\sin\theta_1)^2 = L_2^2 \tag{2}$$

For brevity, $x^* = x + r - R$ is defined. This quantity is equivalent to $X^* = X + R_2 - R_1$ in Pierrot et al. (1990), namely a shift of the reference point so that the difference between the base and end-effector radii is collected in a single variable. Expanding both squared terms in Equation (2) gives

$$x^{*2} - 2L_1x^*\cos\theta_1 + L_1^2\cos^2\theta_1 + y^2 + z^2 + 2L_1z\sin\theta_1 + L_1^2\sin^2\theta_1 = L_2^2 \tag{3}$$

The term $L_1^2 \cos^2\theta_1 + L_1^2 \sin^2\theta_1$ reduces to $L_1^2$ because of the identity $\cos^2\theta_1 + \sin^2\theta_1 = 1$. After collecting the terms containing $\theta_1$ on the left-hand side, an equation of the form $a\cos\theta_1 + b\sin\theta_1 = c$ is obtained:

$$\underbrace{2L_1x^*}_{a}\cos\theta_1 + \underbrace{(-2L_1z)}_{b}\sin\theta_1 = \underbrace{x^{*2} + y^2 + z^2 + L_1^2 - L_2^2}_{c} \tag{4}$$

Equation (4) is equivalent to Equation (4.2) in Pierrot et al. (1990). The difference in signs between the two arises only from the conventions for the direction of the $z$-axis and the positive direction of the angle, while the form of the equation is the same. For a given target point $(x, y, z)$, the values of $a$, $b$, and $c$ are known numbers, so the only unknown quantity is $\theta_1$. Its solution is

$$\theta_1 = \operatorname{atan2}(b, a) - \arccos\left(\frac{c}{\sqrt{a^2+b^2}}\right) \tag{5}$$

Equation (5) has a solution only if $|c| \leq \sqrt{(a^2 + b^2)}$. If this condition is not satisfied, the target point lies outside the workspace. Equation (4) has two solutions, and Pierrot et al. (1990) chose the solution that avoids structural singularities. In this study, the negative sign in Equation (5) was chosen because it yields an outward-pointing elbow configuration that matches the arrangement of the robot.

The same calculation applies to arms 2 and 3, which are located at angles $\varphi_2 = 120°$ and $\varphi_3 = 240°$ relative to the $x$-axis. The target coordinates are first rotated into the working

plane of arm $i$ using Equation (6), and then $x$, $y$, and $\theta_1$ in Equations (2)–(5) are replaced by $x_i$, $y_i$, and $\theta_i$ (Pierrot et al., 1990):

$$x_i = x\cos\varphi_i + y\sin\varphi_i, \qquad y_i = -x\sin\varphi_i + y\cos\varphi_i \tag{6}$$

Equations (1)–(6) form a simplified kinematic model that requires only basic algebraic and trigonometric operations. Thus, the angles of the three arms for each target point can be computed directly by the microcontroller without numerical iteration.

**Conversion of Arm Angle to Microsteps**

The angle obtained from Equation (5) is converted into the number of microsteps sent to the stepper driver. The number of microsteps required for one degree of upper-arm rotation is determined by the motor full-step angle, the microstepping factor, and the belt transmission ratio:

$$k = \frac{\mu G}{\alpha_s} \tag{7}$$

With $a_s$ = 1.8°, $\mu$ = 16, and $G$ = 3, $k$ = 26.67 microsteps per degree is obtained. The number of microsteps for arm $i$ is calculated from the homing position:

$$N_i = \text{round}\left[k\left(\theta_i - \theta_{\text{home},i}\right)\right] \tag{8}$$

The sign of $N_i$ follows the direction of rotation that increases $\theta_i$. The arm angular resolution is $1/k$ = 0.0375° per microstep, so the quantization error due to rounding in Equation (8) is at most 0.01875°. This resolution is a theoretical limit. The actual angular accuracy is also affected by non-uniform microstep positions, transmission backlash, and possible lost steps, whose combined effect is examined through the arm-angle accuracy test.

**Testing Procedure**

The data collection setup for both tests is shown in Figure 5.

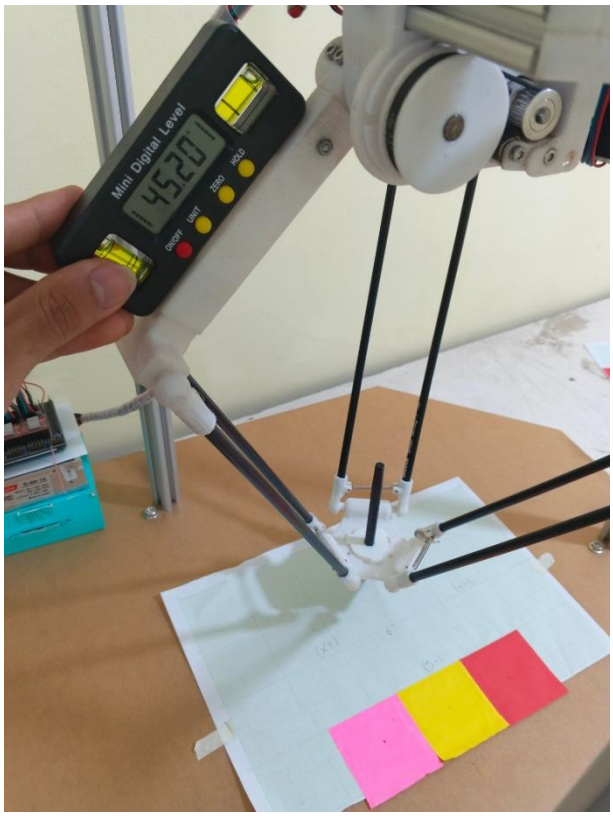



**Figure 5. Data Collection Setup: Reading the Upper-Arm Angle with a Digital Inclinometer and the Work Surface with Millimeter Paper and Three Waste-Bin Position Markers**

Figure 5 shows the digital inclinometer placed on the surface of the upper arm to read the arm angle when the robot is at a test point. Below the end effector, millimeter paper is taped to the base plate as the work surface, with the coordinate axes marked on the paper. Three pink, yellow, and red papers mark the positions of the three waste bins that serve as the accuracy test points.

### *Arm-Angle Accuracy Test*

The accuracy test was performed at three test points representing the positions of three waste bins, namely Point 1 (0, −82, −369) mm, Point 2 (−60, −82, −369) mm, and Point 3 (60, −82, −369) mm. The motion sequence was written in a G-code file beginning with the G28 command for homing and M204 S200 to set the acceleration to 200 mm/s², with a movement speed of 80 mm/s. For each point, the code on the Arduino Mega 2560 computed the angles of the three arms using Equations (1)–(6) and then converted them into microsteps using Equations (7) and (8). After the robot reached the point, the actual angle of each arm was read with a digital inclinometer with a resolution of 0.10° placed on the upper arm and then compared with the angle computed by the code. The measurement was

repeated 10 times at each point, with the robot returning to the standby position between repetitions, yielding 3 points × 3 arms × 10 repetitions = 90 angle data.

***End-Effector Position Precision Test***

The precision test was performed to assess the consistency of the end-effector position over repetitions under the same conditions. A pen was mounted coaxially with the center of the end effector, and millimeter paper was taped to an acrylic base with adhesive tape. The robot was commanded to move to point A (0, 0, −372) mm and point B (0, −82, −372) mm at the same speed and acceleration as in the accuracy test, so that the commanded distance between the two points was 82 mm. At each point, the pen was lowered until it touched the paper and then raised about 10 mm before the robot moved. The test was repeated 10 times with the robot returning to the standby position between repetitions, and the paper was shifted after each repetition so that the pairs of marks from different repetitions did not overlap. The number of 10 repetitions is consistent with precision tests in similar instrumentation studies (Algino et al., 2026; Safitri et al., 2026).

The test paper was scanned at a resolution of 600 dpi, and the ImageJ scale was then set manually based on the millimeter-paper grid at 23.333 pixels/mm, corresponding to a pixel size of 0.0429 mm. The distance between the centers of the marks of point A and point B in each repetition, $D_i$, was then measured using the straight line tool in ImageJ (Schneider et al., 2012). The two marks in one repetition are on the same sheet, so shifting the paper between repetitions does not affect the value of $D_i$.

**Data Analysis Technique**

Accuracy expresses the closeness of a measurement result to the reference value, whereas precision expresses the closeness among repeated measurement results under the same conditions (Joint Committee for Guides in Metrology, 2012). In the accuracy test, the reference value $Y_i$ is the arm angle read by the digital inclinometer as the standard measuring instrument, while $X_i$ is the arm angle computed by the code for the same target point. The percentage accuracy was calculated using Equation (9) (Safitri et al., 2026):

$$\text{Accuracy } (\%) = \left(1 - \left|\frac{Y_i - X_i}{Y_i}\right|\right) \times 100\% \qquad (9)$$

The angular error is expressed as $X_i - Y_i$ in degrees, so a positive error means that the actual arm angle is smaller than the angle computed by the code. The percentage error is the complement of accuracy, namely 100% minus the percentage accuracy, so it does not

require a separate equation. The standard deviation of the inclinometer readings over 10 repetitions is also reported to show the consistency of the arm angle at the same point.

Precision was determined from $n = 10$ measurements of the distance between marks, $D_i$. The mean of all repetitions was calculated using Equation (10), and the percentage precision of each repetition was then calculated using Equation (11) (Algino et al., 2026; Safitri et al., 2026):

$$\bar{X} = \frac{1}{n}\sum_{i=1}^{n} X_i \qquad (10)$$

$$\text{Precision (\%)} = \left(1 - \left|\frac{X_i - \bar{X}}{\bar{X}}\right|\right) \times 100\% \qquad (11)$$

$X_i$ in Equations (10) and (11) is the distance between marks $D_i$ in repetition $i$, and $\bar{X}$ is the mean of all repetitions. The overall precision is expressed as the mean percentage precision of the 10 repetitions. Equation (9) is also used to calculate the distance accuracy, with $Y_i$ being the distance $D_i$ obtained from ImageJ and $X_i$ being the commanded distance between point A and point B. In addition to percentages, the spread of the distances is also expressed in millimeters through the standard deviation $S_D$ and the $\pm 3S_D$ limits, which describe the distance repeatability of the robot.

## RESULTS

### Arm-Angle Accuracy

The accuracy test compared the arm angles computed by the code with the actual arm angles read by the digital inclinometer at three test points. Before the comparison, the angles computed by the code were checked against Equations (1)–(6), and the largest difference was 0.044°, consistent with rounding to multiples of the 0.0375° resolution in Equation (8). A summary of the results from 10 repetitions at each point is presented in Table 2.

**Table 2. Arm-Angle Accuracy at the Three Test Points (n = 10 for Each Arm)**

| Point | Arm | θ code (°) | Mean θ inclinometer ± SD (°) | Mean error (°) | Mean accuracy (%) |
|---|---|---|---|---|---|
| Point 1 | L1 | 46.1625 | 45.80 ± 0.26 | 0.36 | 99.15 |
| Point 1 | L2 | 59.4000 | 58.26 ± 0.19 | 1.14 | 98.04 |
| Point 1 | L3 | 30.8625 | 31.04 ± 0.08 | −0.18 | 99.43 |
| Point 2 | L1 | 60.3750 | 59.41 ± 0.09 | 0.97 | 98.38 |

| Point | Arm | θ code (°) | Mean θ inclinometer ± SD (°) | Mean error (°) | Mean accuracy (%) |
|---|---|---|---|---|---|
| Point 2 | L2 | 57.0000 | 56.10 ± 0.12 | 0.90 | 98.40 |
| Point 2 | L3 | 26.7000 | 26.98 ± 0.04 | −0.28 | 98.96 |
| Point 3 | L1 | 36.0375 | 35.64 ± 0.12 | 0.40 | 98.88 |
| Point 3 | L2 | 66.9375 | 65.22 ± 0.19 | 1.72 | 97.37 |
| Point 3 | L3 | 40.2750 | 40.24 ± 0.08 | 0.04 | 99.81 |
| Mean | – | – | – | – | 98.71 |

Based on Table 2, the mean accuracies of arms 1, 2, and 3 were 98.80%, 97.93%, and 99.40%, respectively, with an overall mean of 98.71%. The highest accuracy was obtained for arm 3 at Point 3, namely 99.81%, whereas the lowest accuracy was obtained for arm 2 at Point 3, namely 97.37%. The standard deviation of the inclinometer readings for each arm was only 0.04–0.26°, or no more than three times the instrument resolution. The spread of errors across all repetitions is shown in Figure 6.

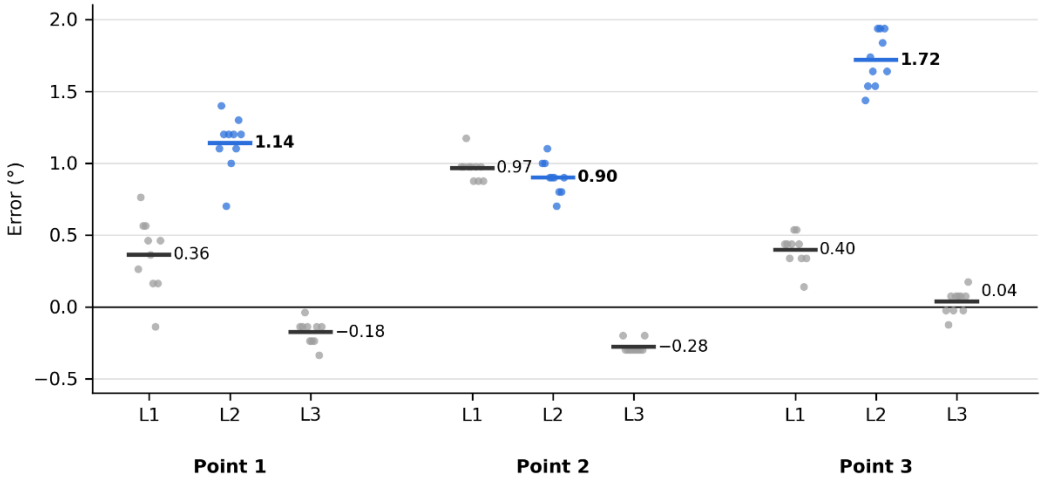



**Figure 6. Arm-Angle Error in Each Repetition at the Three Test Points**

Figure 6 shows that the errors of each arm cluster tightly around their mean values and have the same sign in almost all repetitions. Arms 1 and 2 had positive mean errors at all three points, which means that the actual angles of both arms were smaller than the angles computed by the code. In contrast, the mean error of arm 3 ranged only from −0.28° to 0.04° and changed sign between points. The error of arm 2 also varied with its angle, namely 0.90° at 57.00°, 1.14° at 59.40°, and 1.72° at 66.94°.

The effect of the angular errors on the end-effector position was estimated by finding the position that produces the mean inclinometer angles through a numerical solution of

Equations (2)–(6) and comparing it with the target position. The end-effector position was estimated to shift by 3.9 mm at Point 1, 3.6 mm at Point 2, and 5.8 mm at Point 3, mainly in the positive $y$-direction, while the shift along the $z$-axis was less than 0.1 mm. This estimate assumes that the geometric parameters equal the nominal values in Table 1, so it only indicates the magnitude of the effect of the angular errors and does not replace a direct position measurement.

**End-Effector Position Precision**

The precision test assessed the consistency of the end-effector position over 10 repetitions under the same conditions. The scan of the test paper together with the distance measurements between marks using ImageJ is shown in Figure 7.

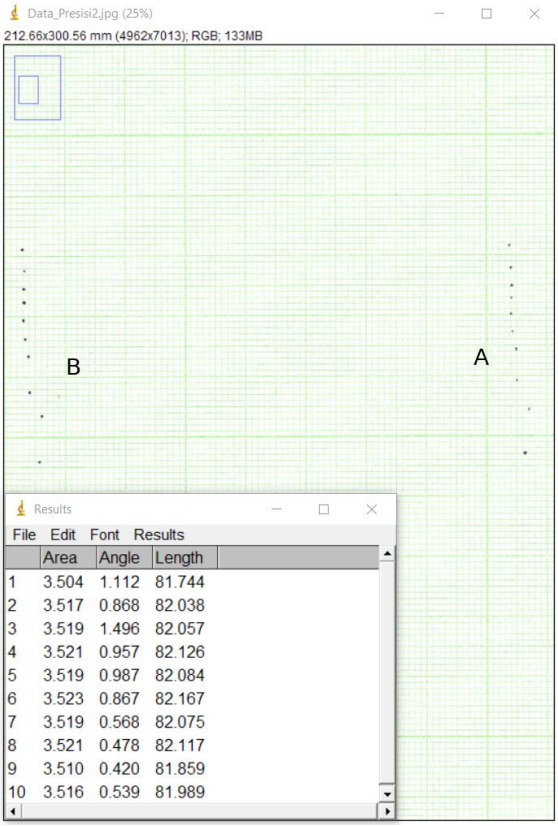



**Figure 7. Scan of the Precision Test Containing Ten Pairs of Pen Marks of Point A and Point B, Together with the Distance Measurements Using ImageJ**

Figure 7 shows ten pairs of pen marks that are separated from one another because the paper was shifted after each repetition. The marks of point A and point B form two columns, so the distance of each pair can be measured without being confused with pairs from other repetitions. The measured distances $D_i$, their deviations from the mean, and the percentage accuracy and precision are presented in Table 3.

**Table 3. Results of the Precision and Distance Accuracy Test Between the Marks of Point A and Point B (Commanded Distance 82 mm, n = 10)**

| Repetition | $D_i$ (mm) | $D_i - D$ (mm) | Accuracy (%) | Precision (%) |
|---|---|---|---|---|
| 1 | 81.744 | −0.282 | 99.69 | 99.66 |
| 2 | 82.038 | 0.012 | 99.95 | 99.98 |
| 3 | 82.057 | 0.031 | 99.93 | 99.96 |
| 4 | 82.126 | 0.100 | 99.85 | 99.88 |
| 5 | 82.084 | 0.058 | 99.90 | 99.93 |
| 6 | 82.167 | 0.141 | 99.80 | 99.83 |
| 7 | 82.075 | 0.049 | 99.91 | 99.94 |
| 8 | 82.117 | 0.091 | 99.86 | 99.89 |
| 9 | 81.859 | −0.167 | 99.83 | 99.80 |
| 10 | 81.989 | −0.037 | 99.99 | 99.96 |
| Mean | 82.026 | – | 99.87 | 99.88 |

Based on Table 3, the distances between marks ranged from 81.744 mm to 82.167 mm, with a mean of 82.026 mm and a standard deviation of 0.131 mm. This mean differed by only 0.026 mm from the commanded distance of 82 mm, with distance accuracy in each repetition between 99.69% and 99.99% and a mean of 99.87%. The precision of each repetition ranged from 99.66% to 99.98%, with a mean precision of 99.88%. When the spread of distances is expressed as ±3 standard deviations, the distance repeatability of the robot is ±0.39 mm. The spread of distances in each repetition is shown in Figure 8.

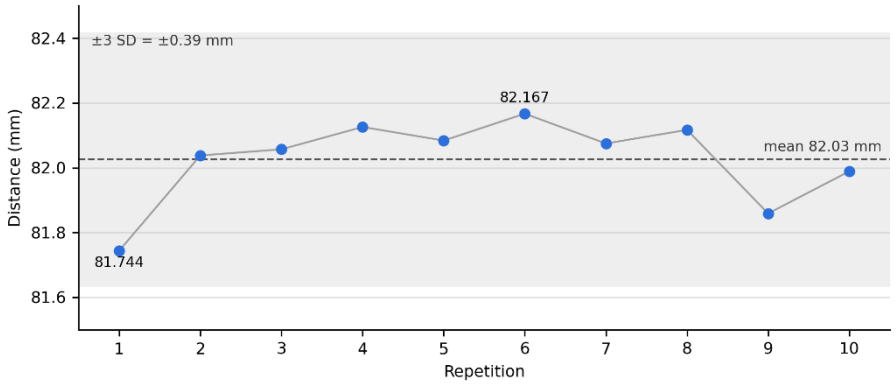



**Figure 8. Distance Between Marks in Ten Repetitions of the Precision Test**

Figure 8 shows that all distances lie within a range of 0.42 mm, or about ten times the pixel size of the scan. The distances did not shift gradually from the first to the last repetition.

## DISCUSSION

The tight clustering of the errors around their mean values indicates that the angular errors are dominated by a systematic component, while the random component is small, which means that the precision of the robot is good. The error of arm 2, which increases with the arm angle, points to factors that depend on the amount of rotation, such as an effective transmission ratio different from 3:1 or belt compliance due to arm loading, so it cannot be explained by the homing reference offset alone. The error of arm 1 does not show a consistent pattern with respect to angle, so its source is more likely a zero-reference offset that has not been fully corrected. Because the errors are systematic and differ for each arm, per-arm compensation has the potential to increase accuracy without modifying the hardware.

The absence of a gradual shift in the distances from the first to the last repetition indicates that no steps were lost and accumulated during testing. The spread of the distances is much smaller than the position shift of 3.6–5.8 mm estimated from the angular errors. Thus, the robot returns to almost the same position in every repetition, whereas the larger error comes from a systematic shift that can be compensated.

The dominance of a systematic error component is consistent with error analyses of Delta mechanisms, in which geometric parameter deviations, joint clearance, and actuator driving errors propagate to the end-effector position (Yang et al., 2021). The angle-dependent error of arm 2 also agrees with measurements on belt-driven positioning systems, in which belt elasticity and micro-slip leave a residual deviation after the motor has reached its commanded position (Tornai et al., 2025). The distance repeatability of ±0.39 mm is larger than the repeatability of about 0.05 mm of the prototype calibrated by Bai et al. (2016) with a laser tracker, which reflects the difference between a stepper-driven belt transmission and a precision prototype. Because the error is systematic, compensation strategies reported for Delta robots, such as correcting the driving angles (Shang et al., 2019) or approximating the inverse kinematics from measured data (Zhao et al., 2023), can be applied directly to the robot in this study.

### Implications for the System

The three test points represent the positions of three waste bins with an opening diameter of 50 mm, so the results of the accuracy test can be used to assess the accuracy of waste placement. The largest end-effector position shift estimated from the angular errors at

the test height is 5.8 mm, which is much smaller than the opening radius of 25 mm. Therefore, the object release point remains within the waste-bin opening even though the systematic errors have not been compensated. However, this shift reduces the space available for the object, so geometrically an object released vertically can only fully enter the bin if its diameter does not exceed about 38 mm. A distance repeatability of ±0.39 mm indicates that the robot motion is consistent, so per-arm angular error compensation is the most effective step to increase this object size limit.

This study has several limitations. Accuracy was tested through the arm angles, while its effect on the end-effector position is still a model-based estimate that assumes the geometric parameters equal their nominal values. The precision test measured the distance between two marks rather than the absolute position relative to the base frame. All tests were also performed at a single height, a single speed setting, and under static unloaded conditions, so the effects of dynamics and conveyor motion have not been covered.

## CONCLUSION

A simplified kinematic model of the Delta robot that maps target coordinates into arm angles and the number of stepper microsteps was formulated and implemented on an Arduino Mega 2560. The angles produced by the code agreed with the model with a difference of no more than 0.044°, which arises only from microstep rounding. Validation against a digital inclinometer at three waste-bin positions yielded a mean angular accuracy of 98.71%, with the highest accuracy for arm 3 at 99.40% and the lowest for arm 2 at 97.93%. The precision test with ten repetitions yielded a mean distance precision of 99.88% and a distance repeatability of ±0.39 mm.

This study contributes a validation procedure for stepper-driven Delta robots that requires only a digital inclinometer, pen marks, and image analysis, and that separates systematic from random errors. The estimated position shift remains within the 25 mm radius of the waste-bin opening, so the robot can place objects at the three tested positions as long as the object diameter does not exceed about 38 mm.

Future work should apply per-arm angular error compensation, particularly for arm 2, whose error increases with the arm angle. The end-effector position should also be measured directly in three dimensions using a measurement scale calibrated against a long

reference length. In addition, the tests should be extended to several heights, speeds, and loaded conditions, including after a suction cup is fitted for waste sorting.

## REFERENCES


Algino, Asrizal, & Kamus, Z. (2026). Analysis of INA219 sensor accuracy and precision for current measurement in a Wheatstone bridge circuit. *Research on Instrumentation, 3*(2), 21–28. https://doi.org/10.66926/rins.2026.1.58

Allegro MicroSystems. (2022, April 5). *A4988: DMOS microstepping driver with translator and overcurrent protection* (4988-DS, Rev. 8). https://www.allegromicro.com/-/media/files/datasheets/a4988-datasheet.pdf

Arbeláez-Estrada, J. C., Vallejo, P., Aguilar, J., Tabares-Betancur, M. S., Ríos-Zapata, D., Ruiz-Arenas, S., & Rendón-Vélez, E. (2023). A systematic literature review of waste identification in automatic separation systems. *Recycling, 8*(6), Article 86. https://doi.org/10.3390/recycling8060086

Bai, P., Mei, J., Huang, T., & Chetwynd, D. G. (2016). Kinematic calibration of Delta robot using distance measurements. *Proceedings of the Institution of Mechanical Engineers, Part C: Journal of Mechanical Engineering Science, 230*(3), 414–424. https://doi.org/10.1177/0954406215603739

Bentaleb, T., & Iqbal, J. (2020). On the improvement of calibration accuracy of parallel robots—Modeling and optimization. *Journal of Theoretical and Applied Mechanics, 58*(1), 261–272. https://doi.org/10.15632/jtam-pl/115863

Cao, L., Liu, J., Zhang, J., Jiang, C., & Zhang, D. (2023). Positioning accuracy reliability analysis of industrial robots considering epistemic uncertainty and correlation. *Journal of Mechanical Design, 145*(2), Article 023303. https://doi.org/10.1115/1.4055926

Clavel, R. (1988). DELTA, a fast robot with parallel geometry. In *Proceedings of the 18th International Symposium on Industrial Robots* (pp. 91–100). IFS Publications.

Creswell, J. W., & Creswell, J. D. (2018). *Research design: Qualitative, quantitative, and mixed methods approaches* (5th ed.). SAGE Publications. https://www.sagepub.com/shop/buy-a-book/research-design-5-255675

Elassal, A., Abdelaal, M., Osama, M., & Elhnidy, H. (2024). Low-cost parallel delta robot for a pick-and-place application with the support of the vision system. *e-Prime—Advances in Electrical Engineering, Electronics and Energy, 8*, Article 100518. https://doi.org/10.1016/j.prime.2024.100518

Fang, B., Yu, J., Chen, Z., Osman, A. I., Farghali, M., Ihara, I., Hamza, E. H., Rooney, D. W., & Yap, P.-S. (2023). Artificial intelligence for waste management in smart cities: A review. *Environmental Chemistry Letters, 21*(4), 1959–1989. https://doi.org/10.1007/s10311-023-01604-3

Joint Committee for Guides in Metrology. (2012). *International vocabulary of metrology—Basic and general concepts and associated terms (VIM)* (3rd ed., JCGM 200:2012). https://doi.org/10.59161/JCGM200-2012

Kılıç, E., Doğruer, C. U., Dölen, M., & Koku, A. B. (2012). Position estimation for timing belt drives of precision machinery using structured neural networks. *Mechanical*

*Systems and Signal Processing, 29*, 343–361. https://doi.org/10.1016/j.ymssp.2011.10.013

Kılıç, E., Dölen, M., & Koku, A. B. (2010). Analysis and estimation of motion transmission errors of a timing belt drive. *Turkish Journal of Electrical Engineering and Computer Sciences, 18*(5), 883–898. https://doi.org/10.3906/elk-0906-44

Kiyokawa, T., Takamatsu, J., & Koyanaka, S. (2024). Challenges for future robotic sorters of mixed industrial waste: A survey. *IEEE Transactions on Automation Science and Engineering, 21*(1), 1023–1040. https://doi.org/10.1109/TASE.2022.3221969

Le, H. P., Vo, D. C., & Thai, T. H. (2023). Design a low-cost Delta robot arm for pick and place applications based on computer vision. *FME Transactions, 51*(1), 99–108. https://doi.org/10.5937/fme2301099P

Lu, W., & Chen, J. (2022). Computer vision for solid waste sorting: A critical review of academic research. *Waste Management, 142*, 29–43. https://doi.org/10.1016/j.wasman.2022.02.009

Lubongo, C., & Alexandridis, P. (2022). Assessment of performance and challenges in use of commercial automated sorting technology for plastic waste. *Recycling, 7*(2), Article 11. https://doi.org/10.3390/recycling7020011

Moon, S., & Kim, D. H. (2014). Step-out detection and error compensation for a micro-stepper motor using current feedback. *Mechatronics, 24*(3), 265–273. https://doi.org/10.1016/j.mechatronics.2014.02.012

Pierrot, F., Reynaud, C., & Fournier, A. (1990). DELTA: A simple and efficient parallel robot. *Robotica, 8*(2), 105–109. https://doi.org/10.1017/S0263574700007669

Pillans, J. (2021). Reducing position errors by vibration optimization of stepper motor drive waveforms. *IEEE Transactions on Industrial Electronics, 68*(6), 5176–5183. https://doi.org/10.1109/TIE.2020.2982123

RepRap. (n.d.). *RAMPS 1.4*. Retrieved October 24, 2026, from https://reprap.org/wiki/RAMPS_1.4

Safitri, V. O., Sari, M. B., & Sudiar, N. Y. (2026). IoT-based oscillation counter using a tracker sensor. *Research on Instrumentation, 3*(2), 10–20. https://rin.resstech.org/index.php/rin/article/view/59

Schneider, C. A., Rasband, W. S., & Eliceiri, K. W. (2012). NIH Image to ImageJ: 25 years of image analysis. *Nature Methods, 9*(7), 671–675. https://doi.org/10.1038/nmeth.2089

Shahria, M. T., Sunny, M. S. H., Zarif, M. I. I., Ghommam, J., Ahamed, S. I., & Rahman, M. H. (2022). A comprehensive review of vision-based robotic applications: Current state, components, approaches, barriers, and potential solutions. *Robotics, 11*(6), Article 139. https://doi.org/10.3390/robotics11060139

Shang, D., Li, Y., Liu, Y., & Cui, S. (2019). Research on the motion error analysis and compensation strategy of the Delta robot. *Mathematics, 7*(5), Article 411. https://doi.org/10.3390/math7050411

Staicu, St., & Carp-Ciocardia, D. C. (2003). Dynamic analysis of Clavel's Delta parallel robot. In *2003 IEEE International Conference on Robotics and Automation* (Vol. 3, pp. 4116–4121). IEEE. https://doi.org/10.1109/ROBOT.2003.1242230

Tornai, T., Simon, J., Gogolák, L., & Fürstner, I. (2025). Accuracy evaluation of a linear servo positioning system. *Actuators, 14*(12), Article 613. https://doi.org/10.3390/act14120613

Yamtuan, K., Radomngam, T., & Prempraneerach, P. (2023). Visual servo kinematic control of Delta robot using YOLOv5 algorithm. *Journal of Robotics and Control (JRC), 4*(6), 818–831. https://doi.org/10.18196/jrc.v4i6.19102

Yang, Q., Ma, H., Ma, J., Sun, Z., & Li, C. (2021). Sensitivity analysis of reliability of low-mobility parallel mechanisms based on a response surface method. *Applied Sciences, 11*(19), Article 9002. https://doi.org/10.3390/app11199002

Zhao, A., Toudeshki, A., Ehsani, R., & Sun, J.-Q. (2023). Data-driven inverse kinematics approximation of a Delta robot with stepper motors. *Robotics, 12*(5), Article 135. https://doi.org/10.3390/robotics12050135